Volume 1 | Number 1 | Jan 2013 | Pages 1–100

Dalton Transactions

An international journal of inorganic chemistry
www.rsc.org/dalton

ROYAL SOCIETY OF CHEMISTRY

ROYAL SOCIETY OF CHEMISTRY

www.rsc.org/dalton

Crystal Structure and Magnetic Properties of a Zintl Phase EuIrIn$_4$: The First Member in the Eu-Ir-In Family

Sumanta Sarkar,[1] Matthias J. Gutmann,[2] Sebastian C. Peter[1]*

[1]New Chemistry Unit, Jawaharlal Nehru Centre for Advanced Scientific Research, Jakkur, Bangalore, 560064, India

[2]ISIS Facility, STFC-Rutherford Appleton Laboratory, Didcot, OX11 OQX, United Kingdom

Abstract. The indium-rich intermetallic compound EuIrIn$_4$ was synthesized using indium as active metal flux. The crystal structure of EuIrIn$_4$ was investigated by X-ray powder and single crystal diffraction. EuIrIn$_4$ crystallizes in the YNiAl$_4$ type, *Cmcm* space group, with lattice parameters, a = 4.5206(9) Å, b = 16.937(3) Å, c = 7.2661(15) Å. Europium atoms in EuIrIn$_4$ are surrounded by three dimensional [IrIn$_4$] polyanionic networks. EuIrIn$_4$ shows two successive antiferromagnetic transitions at 5.4 and 10.8 K. Modified Curie-Weiss fitting on the magnetic susceptibility data within the temperature regions 15-300 K gives the effective magnetic moments 8.45 μ_B/Eu. EuIrIn$_4$ shows pronounced magnetic anisotropy perpendicular to the direction of applied magnetic field.

Key Words: Metal Flux technique, Crystal Growth, Crystallography, Anisotropy, Magnetism.

* Corresponding author. Phone: 080-22082298, Fax: 080-22082627

sebastiancp@jncasr.ac.in (S. C. Peter)

1. Introduction

The chemistry of Zintl phases is a rich subject in materials science and still continues to evolve through different works done by many research groups throughout the world. Zintl phases are ionic intermetallic compounds with a polyanionic covalently bonded network. The narrow band gap semiconducting nature makes it an ideal candidate for thermoelectric applications. Indium, like its other group members such as gallium, thallium, etc. is capable of forming extensive polyanionic clusters, which renders structural diversity in these classes of compounds. Binary and pseudo-binary intermetallic Zintl phases containing indium and alkali/alkaline/rare earth (RE) metals as active components are highly studied for their structural diversity with different geometry ranging from zigzag chains,[1] layered icosahedra[2] to square pyramidal clusters,[3] pentagonal dodecahedra[4] and many other variations in novel bonding[5] and physical characteristics.[6, 7] In some cases, these compounds have been classified as classical Zintl phases. Na_7In_{12},[8, 9] KNa_3In_9,[1] La_3In_5[10] and $SrGeIn$[11] are a few classical examples in this category. However, there are compounds which deviate from Zintl-Klemm concept due to the complexity in structure such as highly packed or condensed indium polyanionic networks, as already pointed out by Palasyuk *et al.*[12]

Na_7In_{12} is constructed by a 16-vertex *closo* indium network, which is an eleven membered *nido* block of indium and two triangular units constructed by indium atoms;[8] KNa_3In_9 is built by a complex layered array of hollow In_{12} icosahedra interconnected by zigzag fashioned In chains[1] and A_3In_5 (A = Y, La) have closed shell *nido* deltahedron structure.[10] Introduction of transition metals into the polyanionic network brings in even more complications in both structural and electronic properties.[12] This trend was verified by our previous work[13] wherein it

was shown schematically that step by step incorporation of transition metal and *p*-block elements (indium) in $EuIn_2$, which crystallizes in simple $CaIn_2$ structure type to the ternary $EuAuIn_2$, followed by $EuAuIn_4$ and finally complex $EuAu_2In_4$. In this process, the cell length not only increases along a particular direction but also enhances the complexity in the packing of the polyindide network. It was further seen that the Eu-Eu bond distances increased in the following order - 3.9250 Å in $EuIn_2$,[14] 4.1246 Å in $EuAuIn_2$,[15] 4.6080(3) Å in $EuAuIn_4$ to 4.6616(2) Å in $EuAu_2In_4$.[13] The increase in bond distance between two adjacent Eu atoms (which is the main magnetic species in these compounds) has substantial effect on the physical properties of the compound. The increase in *RE-RE* distance decreases direct spin coupling between two adjacent atoms and they couple through the itinerant or conduction electrons giving rise to RKKY interaction.[16, 17]

Motivated by our earlier work on $EuAuIn_4$, we initially focused on the synthesis of $EuIrIn_4$ and $EuPtIn_4$. During the progress of our work, we noticed two research groups also worked on $EuPtIn_4$.[18-20] So, we have focused only on $EuIrIn_4$, which is in fact first compound in the Eu-Ir-in family. Here, we report the synthesis, crystal growth and the structural aspects of a new compound $EuIrIn_4$. Well shaped single crystals of $EuIrIn_4$ were obtained from the reactions run in excess indium which has been extensively used in recent years to obtain large single crystals of intermetallic compounds.[13, 21-37] The crystal structure of the compounds was deduced from the single crystal X-ray diffraction data. Interestingly, $EuIrIn_4$ crystallize in the $YNiAl_4$ type structure, which is unexpected due to the common trend of the group 9 transition metals favored the $LaCoAl_4$ type structure. The structural aspects between the compounds $EuIrIn_4$ and $SrIrIn_4$ ($LaCoAl_4$ type structure) are compared and discussed in detail. We also briefly discuss about the bulk and anisotropic magnetic properties of $EuIrIn_4$.

3

2.1. Synthesis

Europium (ingots, 99.99%, ESPI metals), iridium (powder, 99.99%, Alfa Aesar) and indium (tear drops, 99.99%, Alfa Aesar) were used as purchased without any further purification. 3 mmol of europium, 2 mmol of iridium and 30 mmol of indium were taken in an alumina crucible under an inert (argon) atmosphere inside a glove box (H_2O, O_2 levels <0.1 ppm). The purpose of excess indium is to act as an active metal flux. The crucible was placed in a 13 mm quartz tube and was flame-sealed under vacuum of 10^{-6} torr, to prevent oxidation during heating. The tube was then placed in a vertical tube furnace and was heated to 1273 K in 10 h, kept at that temperature for 6 h. The temperature was then lowered down to 1123 K in 2 h and annealed at this temperature for 72 h. Finally, the system was allowed to cool slowly to room temperature in 48 h. The reaction products were isolated from the excess In flux by heating at 623 K and subsequent centrifugation through a coarse frit. The remaining flux was removed by immersion and sonication in glacial acetic acid for 24 h. The final crystalline product were rinsed with water and dried with acetone in a vacuum oven at 350 K for 12 h. The compound $EuIrIn_4$ was grown as shiny thin long plate shaped crystals with an average length of 4-5 mm. The single crystals were insensitive to air and moisture with no decomposition observed even after several months. The compound was obtained in ~80% yield with $EuIn_2$ as the major impurity phase. Single crystals were carefully selected for the elemental analysis, structure characterization and the magnetic measurements. Attempts to synthesize bulk compounds by high frequency induction heating were not successful.

2.2. Powder X-Ray Diffraction. The phase identity and purity of $EuIrIn_4$ was determined by powder X-ray diffraction technique. The data was collected at room temperature

on a Rigaku Miniflex with Cu-K$_\alpha$ X-ray source (λ = 1.5406 Å), equipped with a scintillation

counter detector in the angular range $25^o \leq 2\theta \leq 70^o$ with the step size 0.02^o and scan rate of 1

s/step. The experimental patterns were compared to the pattern calculated from the single crystal

structure refinement. The comparison of the powder patterns with the simulated pattern obtained

from the single crystal data is shown in Figures 1S in the supporting information.

2.3. Elemental Analysis. Quantitative microanalysis on EuIrIn$_4$ was performed with a

FEI NOVA NANOSEM 600 instrument equipped with an EDAX® instrument. Data were

acquired with an accelerating voltage of 20 kV and a 100 s accumulation time. Typical metallic

rod and plate shaped single crystals of EuIrIn$_4$ obtained from the flux method are shown in

Figure 1. The EDAX analysis was performed using P/B-ZAF standardless method (where, Z =

atomic no. correction factor, A = absorption correction factor, F = fluorescence factor, P/B =

peak to background model) on visibly clean surfaces of the crystals. The microanalysis on

different spots on the crystal gave an average molar composition of 18.7% Eu, 15.3% Ir and 66%

In is very close to the composition obtained from X-ray diffraction on single crystals.

2.4. Single Crystal X-Ray Diffraction. A carefully selected single crystal of EuIrIn$_4$ was

mounted on a thin glass fiber. X-ray single crystal structural data for EuIrIn$_4$ were collected at

100 K on an Oxford Diffraction Supernova diffractometer equipped with an ATLAS CCD

detector. Mo-Kα radiation with a wavelength of λ = 0.71073 Å operating at 50 kV and 30 mA.

with the ω scan mode using a full sphere of 60 frames acquired up to 91.2° in 2θ. The individual

frames were measured with steps of 0.50° and an exposure time of 40 s per frame at temperatures

293 K and 100 K. A crystal of suitable size (0.2 x 0.1 x 0.07 mm^3) was cut from a rod-shaped

crystal and mounted on a thin glass (~0.1 mm) fiber with commercially available super glue.

Data were processed using Crysalis Pro and an analytic absorption correction was applied using a face-indexation of the crystal. The crystal structure were solved by SHELXS 97[38] and refined by full matrix least-squares method using SHELXL.[39] Diamond (version, 3.2g) was used for generating packing diagrams.[40]

2.5. Structure Refinement

The preliminary data analysis suggested that EuIrIn$_4$ is a *C*-centered orthorhombic crystal system and *mmm* Laue class. The lattice parameters obtained are a = 4. 4.5206(9) Å, b = 16.937(3) Å, c = 7.2661(15) Å were compatible with the YNiAl$_4$ structure type. EDAX data also hinted a rough composition (atomic weight %) of 1:1:4 for Eu:Ir:In. Therefore, the atomic coordinates of YNiAl$_4$ were taken as a model and the structures were refined using SHELXL-97 (full-matrix least-squares on F^2)[39] with anisotropic atomic displacement parameters for all atoms. The occupancy parameters were refined in a separate series of least-squares cycles in order to check the correct composition. It was noted that the data collected at high exposure time (40s/frame) owing to the high absorption cross-section of Ir. Due to the unusual displacement parameter for In1 for the data at room temperature, we had to collect the data at low temperature (100 K) for EuIrIn$_4$. Finally, the resulting atomic displacement parameters of all positions became well-behaved and the final difference maps showed residuals that were reasonably acceptable. The final compositions obtained from single crystal XRD data corroborate well with EDAX data.

The data collection and refinement parameters for EuIrIn$_4$ are summarized in Table 1. The atomic coordinates and equivalent atomic displacement parameters, anisotropic atomic displacement parameters and important bond lengths are listed in Tables 2, 3 and 4, respectively.

2.6. Magnetic Measurements. Magnetic measurements were performed on selected single crystals of $EuIrIn_4$ arranged in randomly oriented fashion using a Quantum Design Magnetic Property Measurement System - Superconducting Quantum Interference Device (MPMS-SQUID) dc magnetometer. Temperature dependent magnetization data were collected in the field cooled mode (FC) in the temperature range 2 to 300 K at an applied magnetic field of 1000 Oe. Field dependent magnetization data were collected at 300 and 2 K for $EuIrIn_4$ with field sweeping from −60 kOe to 60 kOe. For anisotropic studies, the single crystal was mounted with the help of a plastic straw in the perpendicular and parallel direction of applied field and the magnetic susceptibility was measured against temperature in the range of 2-300 K.

3. Results and Discussion

3.1. Crystal Structure. Compounds with the general formula $RETX_4$ crystallize mainly in the $LaCoAl_4$ and $YNiAl_4$ structure types. It has been observed that the $RETX_4$ compounds with transition metals from group 9 (Co, Rh, Ir) adopt the former structure type[15, 41, 42] except $ThCoGa_4$ (adopts $YNiAl_4$ type),[43] whereas group other transition metals (Ni, Pd, Pt) mostly adopt the $YNiAl_4$ type[13, 15, 42, 44-51] (since large number of $RETX_4$ compounds are reported, only the references for $RETIn_4$ are cited). This kind of switch over from one structure type to another may be caused by (i) size restrictions imposed by the transition metal, (ii) the valence electron count (VEC), and (iii) different bonding characteristics between T and In.

$EuIrIn_4$ is the first intermetallic compound reported in Eu-Ir-In series. Unlike the other group 9 transition metal containing compounds having general formula $RETX_4$, which generally crystallize in the $LaCoAl_4$ type ($a = 7.701$, $b = 4.082$, $c = 7.023$ Å) with *Pmma* space group, $EuIrIn_4$ crystallizes in the orthorhombic $YNiAl_4$ structure type ($a = 4.5206(9)$ Å, $b = 16.937(3)$ Å, $c = 7.2661(15)$ Å) with *Cmcm* space group. It has been described in the previous literature

that $RETX_4$, with T = Au, Ir, Pt compounds have low valence electron count $(VEC)^{12}$ due to electron deficient transition metals with high relativistic effects[52, 53] causing shrinkage in cell volume and shorter homoatomic as well as heteroatomic (X-X and T-X) bond distances. This argument, however, does not hold in case of $EuTIn_4$ (T = Au, Ir, Pt) series of compounds as all of these crystallize in *Cmcm* space group with a cell volume approximately double of the primitive counterpart belonging to *Pmma* space group. The crystal structure of $EuIrIn_4$ is shown in Figure 2. The structure can be described as Eu atoms are embedded in the pentagonal $[IrIn_4]$ networks separated by two different kinds of tetrameric networks; one of these is a puckered zig-zag $[Ir_2In_2]$ layer (Figure 2b) and another puckered $[In]_4$ tetrameric network (Figure 2c and 2d). In view of the previously studied compounds, e.g. $CaPdIn_4,^{42}$ $LaNiIn_4,^{54}$ etc. which crystallize in *Cmcm* space group, the present compounds can also be described in terms of Zintl concept with a formula $Eu^{2+}[irIn4]^{2-}$. The divalent nature of Eu was evident from both crystallographic as well as magnetic data as discussed in the next section.

At this point, it is worthwhile to compare the structures of $EuIrIn_4$ and $SrIrIn_4^{41}$ geometrically, the later crystallizes in the $LaCoAl_4$ structure type. The representative structures of these two compounds are shown in Figure 3a and 3b, respectively. As a matter of fact, both the structures are built up by zig-zag ribbons of tetrameric and trimeric units of $[IrIn_4]$, but the main difference is in the way they are arranged. In case of the *c*- centered structure i.e. for $EuIrIn_4$, there are two kinds of arrangements; one is propagated along the *c*- axis and another is arranged along the two diagonals of the *bc*– plane and these two diagonal ribbons are tangled or interconnected at every triangular unit. The primitive structure, $SrIrIn_4$ is however simpler where the ribbons are propagated along the *a* –axis parallelly separated by $[Ir_2In_3]$ pentagonal structures and do not cross each other. These two structures can also be compared crystallographically by

symmetric reduction shown in Figure 4. The non-centrosymmetric space group, *Pmma* can be deduced from centrosymmetric *Cmcm* space group by a simple klassengleichen (*k*) operation of index 2 followed by a shift of origin to (0, 1/2, 0). This removes the center of symmetry rendering the unit cell to primitive orthorhombic. The coordination environments of each atom in both structures have been compared side by side in Figure 5. The two compounds differs only in terms of the coordination environment of the central atom i.e. Eu and Sr, respectively, for $EuIrIn_4$ and $SrIrIn_4$. Eu resides in a distorted pseudo Frank-Kasper type cage ($Eu_2In_{13}Ir_2$) which is equivalent to a hexagonal bipyramidal structure, Sr on the other hand, resides in open type 15-membered Frank-Kasper cage ($IrIn_{12}Sr_2$). All the In atoms, namely In(1), In(2) and In(3) in both compounds have cubooctahedron type coordination polyhedral (CP) with a coordination number of 12. The transition metal, i.e. Ir has tricapped trigonal prismatic CP in both compounds. This observation clearly establishes that low valence electron count and the size effect of the transition metal is not sufficient criteria for dense crystal packing giving rise to *Pmma* space group. The reason for this anomalous behavior is unknown to us and urges further theoretical as well as experimental studies. It is also worthwhile to discuss the bonding characteristics in the crystal structure of $EuIrIn_4$. Ir-In bond distance range from 2.6109(11) to 2.6804(7) Å, which is slightly shorter than the covalent bond length of Ir-In (2.83 Å)[55] hinting towards strong bonding interactions between Ir and In. The In-In distance varies in a wide range 2.9813(12) - 3.1628(8) Å suggests considerable distortion in the In cubes which are the basic structural unit in $EuIrIn_4$. The Eu-Eu bond distance 4.5206(9) is comparable to the Eu-Eu bond distances in compounds with divalent Eu moiety in other intermetallic compounds like $EuCu_2Si_2$ and $EuGe_2$,[56-58] which corroborate with the magnetic measurements as well.

3.2. Magnetism

The molar magnetic susceptibility of randomly oriented single crystals of $EuIrIn_4$ was measured in an applied field of 1 kOe (Figure 6a). The plot exhibits a sharp peak around 5.4 K (T_{N1}) indicating antiferromagnetic phase transition followed by another broad hump at around 10.8 K (T_{N2}) which corresponds to another probable antiferromagnetic transition. Above T_{N2}, the χ (T) falls rather sharply and decreases with increasing temperature. The plot of inverse susceptibility (χ^{-1}) as a function of temperature deviates substantially from linearity and hence was fitted with the modified Curie-Weiss in the temperature range 15-300 K. The curve became linear above T_{N2} after subtracting the residual magnetic susceptibility (χ_o = -0.011 emumol^{-1}). The fitting gives the value of paramagnetic Curie temperature (θ_p) of -18.7 K and an effective magnetic moment (μ_{eff}) of 8.45 μ_B/Eu. The value of μ_{eff} is abnormally higher than the expected free ion moment of divalent Eu (7.94 μ_B), and can be attributed to factors such as conduction electron polarization.[59] This kind of high magnetic moment over spin only moment is not common, but it was observed in other rare earth based compounds as for example in Tb_2CuGe_3.[59] Figure 6b shows the magnetization of the sample while varying the magnetic field on the same sample. Above the ordering temperature (300 K), the magnetic moment varies almost linearly with applied field hinting toward the fact that at this temperature the Eu moments hardly order with applied magnetic field and do not saturate even up to the highest attainable field. Below the ordering temperature (2 K) the compound shows weak metamagnetic transition below a critical field (20 kOe). This could be because of sudden spin flopping towards the applied magnetic field. This kind of transition is often encountered in many Eu containing intermetallic compounds which order antiferromagnetically below a critical temperature (T_N).[60, 61]

The magnetic susceptibility, χ, on the single crystal of $EuIrIn_4$ has been measured in two orientations, one being parallel to the applied magnetic field (marked as H || *a*-axis) and other

being perpendicular to the field (marked as H $\perp$ a-axis) (Figure 7). In both measurements, χ increases gradually with increasing temperature and undergoes magnetic ordering (T$_N$) around 11 K. The χ falls rapidly above 11 K with increasing temperature up to 200 K (Figure 7 shows only upto 30 K for better clarity) and then decreases marginally. The anisotropy between the perpendicular and the parallel directions of the single crystal is clearly evident from Figure 7. Below 11 K, it is seen that the behavior of χ(T) for both directions is slightly different in terms of the value of χ at the lowest temperature. For H $\perp$ a-axis, χ tends to demagnetize at low temperature whereas for H $\parallel$ a χ saturate at the higher value.

4. Conclusion. Metal flux technique has been used as an efficient method for the crystal growth of a new compound EuIrIn$_4$, which is in fact first member in the Eu-Ir-In family. The X-ray diffraction data on selected single crystals of EuIrIn$_4$ suggest that it crystallizes in the centrosymmetric *Cmcm* space group, which contradicts the conventional trend of compounds with group 9 elements which crystallize normally in the primitive *Pmma* space group with a half cell volume. For this reason, we have compared the structures of EuIrIn$_4$ and SrIrIn$_4$, later one crystallize in the *Pmma* space group. Our findings on the structure of EuIrIn$_4$ hints that *Cmcm* is likely to be the most probable space group for all the RETX$_4$ series of compounds in place of *Pmma* space group as the latter space group can be arrived at by removal of the weak superstructure reflections. Another possible reason for this might be the way of synthesis and crystal growth. Most of the previously reported compounds were synthesized by arc melting or high frequency induction heating. On the contrary, metal flux method one of the best techniques to grow well shaped single crystals, which in most of the cases give better superstructure reflections in XRD. These remarks however call for a thorough experimental as well as theoretical investigations and remain open for further studies.

Electronic Supplementary Information (ESI): Powder X-ray diffraction and crystallographic information files (CIF). The CCDC reference number for EuIrIn$_4$ is CCDC 988634.

Dalton Transactions Accepted Manuscript

References

1. B. Li and J. D. Corbett, *Inorg. Chem.*, 2002, **41**, 3944-3949.

2. J. G. Mao, J. Goodey and A. M. Guloy, *Inorg. Chem.*, 2004, **43**, 282-289.

3. F. Zurcher, R. Nesper, S. Hoffmann and T. F. Fässler, *Z. Anorg. Allg. Chem.*, 2001, **627**, 2211-2219.

4. J. T. Zhao and J. D. Corbett, *Inorg. Chem.*, 1994, **33**, 5721-5726.

5. H. Schäfer, B. Eisenmann and W. Müller, *Angew. Chem. Int. Ed.*, 1973, **12**, 694–712.

6. S. M. Kauzlarich, S. R. Brown and G. J. Snyder, *Dalton Trans.*, 2007, 2099-2107.

7. F. Gascoin, J. Rasmussen and G. J. Snyder, *J. Alloys Compd.*, 2007, **427**, 324-329.

8. S. C. Sevov and J. D. Corbett, *Inorg. Chem.*, 1992, **31**, 1895–1901.

9. T. F. Fässler and S. Hoffmann, *Inorg. Chem.*, 2003, **42**, 5474-5476.

10. J.-T. Zhao and J. D. Corbett, *Inorg. Chem.*, 1995, **34** 378-383.

11. J. G. Mao, J. Goodey and A. M. Guloy, *Inorg. Chem.*, 2002, **41**, 931-937.

12. A. M. Palasyuk and J. D. Corbett, *Inorg. Chem.*, 2008, **47**, 9344-9350.

13. S. Sarkar, M. J. Gutmann and S. C. Peter, *Cryst. Growth Des.*, 2013, **13**, 4285-4294.

14. S. P. Yatsenko, A. A. Semyannikov, K. O. Shakarov and E. G. Fedorova, *J. Less Common Met.*, 1983, **90**, 95-108.

15. R. D. Hoffmann, R. Pöttgen, V. I. Zaremba and Y. M. Kalychak, *Z. Naturforsch. B*, 2000, **55**, 834-840.

16. M. C. Francisco, C. D. Malliakas, R. T. Macaluso, J. Prestigiacomo, N. Haldolaarachchige, P. W. Adams, D. P. Young, Y. Jia, H. Claus, K. E. Gray and M. G. Kanatzidis, *J. Am. Chem. Soc.*, 2012, **134**, 12998-13009.

17. S. Sarkar and S. C. Peter, *Inorg. Chem.*, 2013, **52**, 9741-9748.

18. P. Kushwaha, in *Strongly Corelated Electron Systems (SCES-2013)*, 2013.

19. P. Rosa, T. Grant, C. Jesus, M. Piva, P. Pagliuso and Z. Fisk, in *APS MAR14 Meeting*, The American Physical Society, USA, 2014.

20. P. Kushwaha, A. Thamizhavel, A. K. Nigam and S. Ramakrishnan, *Cryst. Growth Des.*, 2014, **In Press**, 10.1021/cg401864p.

21. U. Subbarao, A. Sebastian, S. Rayaprol, C. S. Yadav, A. Svane, G. Vaitheeswaran and S. C. Peter, *Cryst. Growth Des.*, 2013, **13**, 352-359.

22. U. Subbarao and S. C. Peter, *J. Chem. Sci.*, 2013, **125**, 1315-1323.

23. M. Chondroudi, S. C. Peter, C. D. Malliakas, M. Balasubramanian, Q. A. Li and M. G. Kanatzidis, *Inorg. Chem.*, 2011, **50**, 1184-1193.

24. S. C. Peter, M. Chondroudi, C. D. Malliakas, M. Balasubramanian and M. G. Kanatzidis, *J. Am. Chem. Soc.*, 2011, **133**, 13840-13843.

25. S. C. Peter and M. G. Kanatzidis, *Z. Anorg. Allg. Chem.*, 2012, **638**, 287-293.

26. S. C. Peter, S. Sarkar and M. G. Kanatzidis, *Inorg. Chem.*, 2012, **51**, 10793-10799.

27. S. Sarkar and S. C. Peter, *J. Alloys Compd.*, 2012, **124**, 1385-1390.

28. U. Subbarao and S. C. Peter, *Inorg. Chem.*, 2012, **51**, 6326-6332.

29. S. C. Peter, C. D. Malliakas and M. G. Kanatzidis, *Inorg. Chem.*, 2013, **52**, 4909-4915.

30. S. Sarkar, M. J. Gutmann and S. C. Peter, *Crystengcomm*, 2013, **15**, 8006-8013.

31. J. R. Salvador, J. R. Gour, D. Bilc, S. D. Mahanti and M. G. Kanatzidis, *Inorg. Chem.*, 2004, **43**, 1403-1410.

32. J. R. Salvador, D. Bilc, J. R. Gour, S. D. Mahanti and M. G. Kanatzidis, *Inorg. Chem.*, 2005, **44**, 8670-8679.

33. J. R. Salvador and M. G. Kanatzidis, *Inorg. Chem.*, 2006, **45**, 7091-7099.

34.   J. R. Salvador, K. Hoang, S. D. Mahanti and M. G. Kanatzidis, *Inorg. Chem.*, 2007, **46**, 6933-6941.

35.   V. I. Zaremba, U. C. Rodewald and R. Pöttgen, *Z. Naturforsch. B*, 2003, **58**, 805-808.

36.   S. C. Peter, U. Subbarao, S. Sarkar, G. Vaitheeswaran, A. Svane and M. G. Kanatzidis, *J. Alloys Compd.*, 2014, **589**, 405-411.

37.   M. G. Kanatzidis, R. Pöttgen and W. Jeitschko, *Angew. Chem. Int. Ed.*, 2005, **44**, 6996-7023.

38.   G. M. Sheldrick, *Acta Crystallogr. A*, 2008, **64**, 112-122.

39.   G. M. Sheldrick, in *SHELXTL, Program for Crystal Structure Refinement*, University of Göttingen, Göttingen, Germany, 1997.

40.   Diamond, in *version 3.0g, Crystal Impact*, Rathausgasse, Bonn, Germany, 2011.

41.   I. R. Muts, V. I. Zaremba and R. Pöttgen, *Z. Anorg. Allg. Chem.*, 2007, **633**, 2234-2237.

42.   R. D. Hoffmann and R. Pöttgen, *Chem. Eur. J.*, 2000, **6**, 600-607.

43.   R. Wawryk, J. Stepien-Damm, Z. Henkie, T. Cichorek and F. Steglich, *J. Phys-Condens. Mat.*, 2004, **16**, 5427-5434.

44.   K. M. Poduska, F. J. DiSalvo and V. Petricek, *J. Alloy Compd.*, 2000, **308**, 64-70.

45.   S. N. Nesterenko, A. L. Tursina, D. V. Shtepa, H. Noel and Y. D. Seropegin, *J. Alloy Compd.*, 2007, **442**, 93-95.

46.   R. Pottgen, R. Mullmann, B. D. Mosel and H. Eckert, *J. Mater. Chem.*, 1996, **6**, 801-805.

47.   Y. M. Kalychak, V. M. Baranyak, V. I. Zaremba, P. Y. Zavalij, O. V. Dmytrakh and V. A. Bruskov, *Kristallografica*, 1988, **33**, 1017-1018.

48.   I. Muts, V. I. Zaremba, V. V. Baran and R. Pottgen, *Z. Naturforsch B*, 2007, **62**, 1407-1410.

49.   Y. V. Galadzhun and R. Pottgen, *Z. Anorg. Allg. Chem.*, 1999, **625**, 481-487.

50.   V. I. Zaremba, U. C. Rodewald, R. D. Hoffmann, Y. M. Kalychak and R. Pottgen, *Z. Anorg. Allg. Chem.*, 2003, **629**, 1157-1161.

51.   L. V. Sysa and Y. M. Kalychak, *Kristallografica*, 1993, **38**, 271-274.

52.   P. Pyykkö, *Chem. Rev.*, 1998, **88**, 563-594.

53.   P. Pyykkö, *Angew. Chem. Int. Ed.*, 2002, **41**, 3573-3578.

54.   Y. M. Kalychak, V. I. Zaremba, Y. V. Galadzhun, K. Y. Miliyanchuk, R. D. Hoffmann and R. Pöttgen, *Chem. Eur. J.*, 2001, **7**, 5343-5349.

55.   J. Emsley, Clarendon Press, Oxford, 1989.

56.   Y. Takigawa, S. Noguchi and K. Okuda, *J. Magn. Magn. Mater.*, 1988, **76–77**, 345– 346.

57.   P. G. Pagliuso, J. L. Sarrao, J. D. Thompson and M. F. Hundley, *Phys. Rev. B*, 2001 **63**, 092406.

58.   S. Bobev, E. D. Bauer, J. D. Thompson, J. L. Sarrao, G. J. Miller, B. Eck and R. Dronskowski, *J. Solid State Chem.*, 2004, **177**, 3545–3552.

59.   S. Majumdar and E. V. Sampathkumaran, *Solid State Commun.*, 2001, **117**, 645-648.

60.   Y. Hiranaka, A. Nakamura, M. Hedo, T. Takeuchi, A. Mori, Y. Hirose, K. Mitamura, K. Sugiyama, M. Hagiwara, T. Nakama and Y. Onuki, *J. Phys. Soc. Jpn.*, 2013, **82**, 083708.

61.   Z. Hossain, O. Trovarelli, C. Geibel and F. Steglich, *J. Alloys Compd.*, 2001, **323**, 396-399.

Tables

Table 1. Crystal data and structure refinement for EuIrIn$_4$.

Empirical formula	EuIrIn$_4$
Formula weight	803.44
Wavelength	0.71073 Å
Crystal system	Orthorhombic
Space group	*Cmcm*
Temperature	100.00(10) K
Unit cell dimensions	a = 4.5206(9) Å, b = 16.937(3) Å, c = 7.2661(15) Å
Volume	556.32(19) Å^3
Z	4
Density (calculated)	9.593 g/cm^3
Absorption coefficient	51.064 mm^{-1}
F(000)	1344
Crystal size	0.2 x 0.1 x 0.07 mm^3
θ range for data collection	3.7 to 45.6°
Index ranges	-8<=h<=9, -33<=k<=34, -14<=l<=12
Reflections collected	7237
Independent reflections	1338 [R$_{int}$ = 0.0777]
Completeness to θ = 49.40°	99.4%
Refinement method	Full-matrix least-squares on F^2
Data / restraints / parameters	1338 / 0 / 24
Goodness-of-fit	1.055
Final R indices [>2σ(I)]	R$_{obs}$ = 0.0367, wR$_{obs}$ = 0.0689
R indices [all data]	R$_{all}$ = 0.0513, wR$_{all}$ = 0.0773
Extinction coefficient	0.00154(8)
Largest diff. peak and hole	6.207 and -7.003 e·Å^{-3}

[a]$R = \Sigma||F_o|-|F_c|| / \Sigma |F_o|$, $wR = \{\Sigma[w(|F_o|^2 - |F_c|^2)^2] / \Sigma[w(|F_o|^4)]\}^{1/2}$ and calc. $w=1/[\sigma^2(Fo^2)+(0.0613P)^2+42.3592P]$ where $P=(Fo^2+2Fc^2)/3$

Table 2. Atomic coordinates (x10^4) and equivalent isotropic displacement parameters (Å^{2}x10^3) for EuIrIn$_4$ with estimated standard deviations in parentheses.

Label	Wyck. No.	x	y	z	Occupancy	U_{eq}*
Eu	4c	0	3748(1)	2500	1	5(1)
Ir	4c	0	7190(1)	2500	1	5(1)
In(1)	8f	0	1858(1)	448(1)	1	5(1)
In(2)	4c	0	5650(1)	2500	1	6(1)
In(3)	4a	0	0	0	1	7(1)

*U_{eq} is defined as one third of the trace of the orthogonalized U_{ij} tensor.

Table 3. Anisotropic displacement parameters (Å^{2}x10^3) for EuIrIn$_4$ with estimated standard deviations in parentheses.

Label	U_{11}	U_{22}	U_{33}	U_{12}	U_{13}	U_{23}
Eu	4(1)	5(1)	6(1)	0	0	0
Ir	5(1)	6(1)	5(1)	0	0	0
In(1)	3(1)	7(1)	4(1)	0	0	0(1)
In(2)	6(1)	5(1)	8(1)	0	0	0
In(3)	6(1)	5(1)	10(1)	0	0	-1(1)

The anisotropic displacement factor exponent takes the form: $-2\pi^2[h^2a^{*2}U_{11} + ... + 2hka^*b^*U_{12}]$.

Table 4. Bond lengths [Å] for EuIrIn$_4$ with estimated standard deviations in parentheses.

Label	Distances	Label	Distances
Eu(1)-In(2)	3.2201(12)	Ir(1)-In(2)	2.6109(11)
Eu(1)-In(1)#1	3.2791(6)	In(1)-In(1)#7	2.9813(12)
Eu(1)-Ir(1)#5	3.4733(7)	In(1)-In(3)#4	3.1628(8)
Eu(1)-In(3)#2	3.5918(5)	In(2)-In(3)#9	3.1016(5)
Ir-In(1)#10	2.6804(7)		

Symmetry transformations used to generate equivalent atoms:
(1) -x-1/2,-y+1/2,-z (2) -x+1/2,-y+1/2,z+1/2 (3) -x-1/2,-y+1/2,z+1/2 (4) -x+1/2,-y+1/2,-z (5) x-1/2,y-1/2,z (6) x+1/2,y-1/2,z (7) x,y,-z+1/2 (8) x+1/2,y+1/2,z (9) x-1/2,y+1/2,z (10) -x,-y+1,z+1/2 (11) -x,-y+1,-z (12) x+1/2,y+1/2,-z+1/2 (13) x-1/2,y+1/2,-z+1/2 (14) -x,-y,-z (15) -x,-y+1,-z+1

Figures
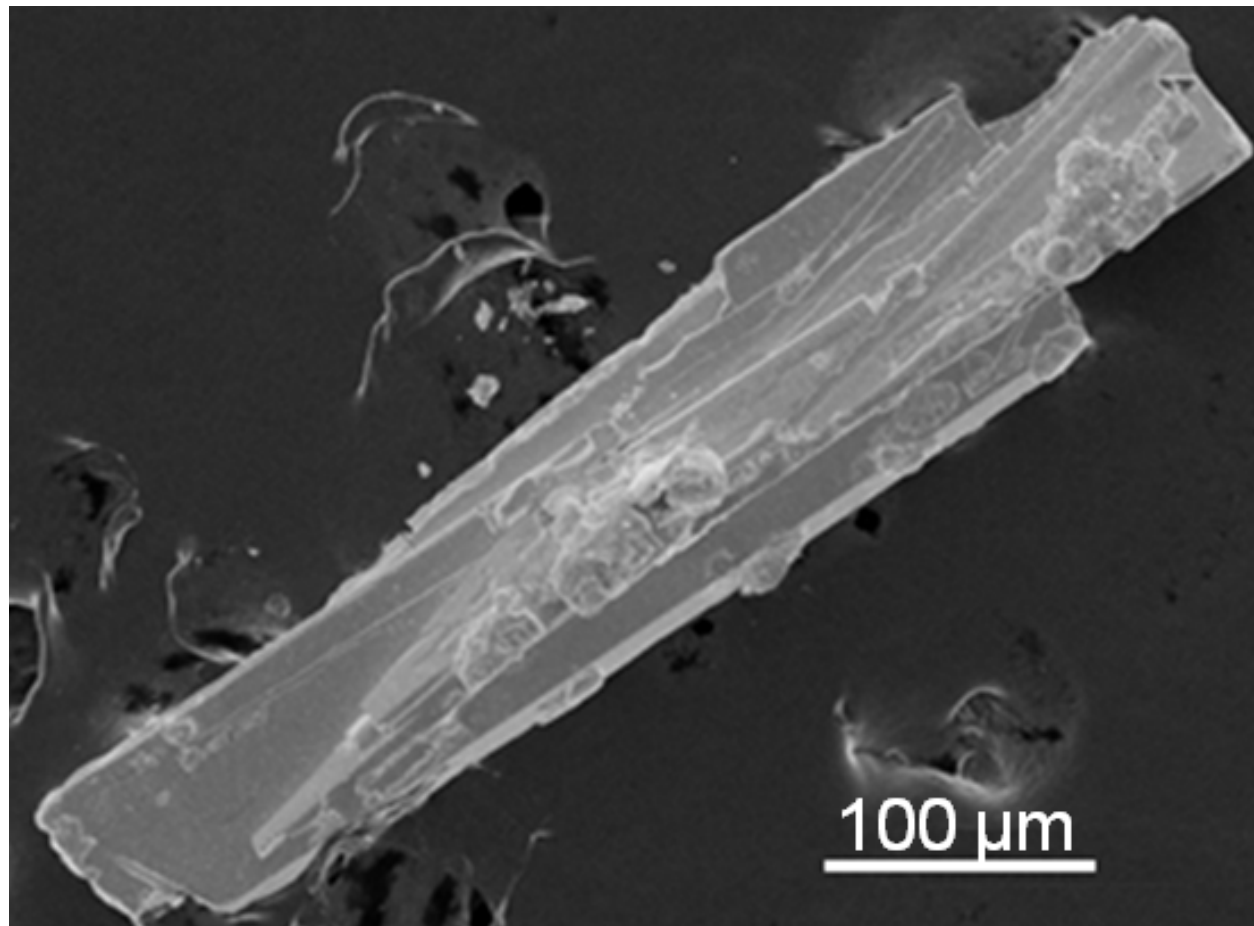
Fig. 1 SEM images of typical single crystals of EuIrIn$_4$.
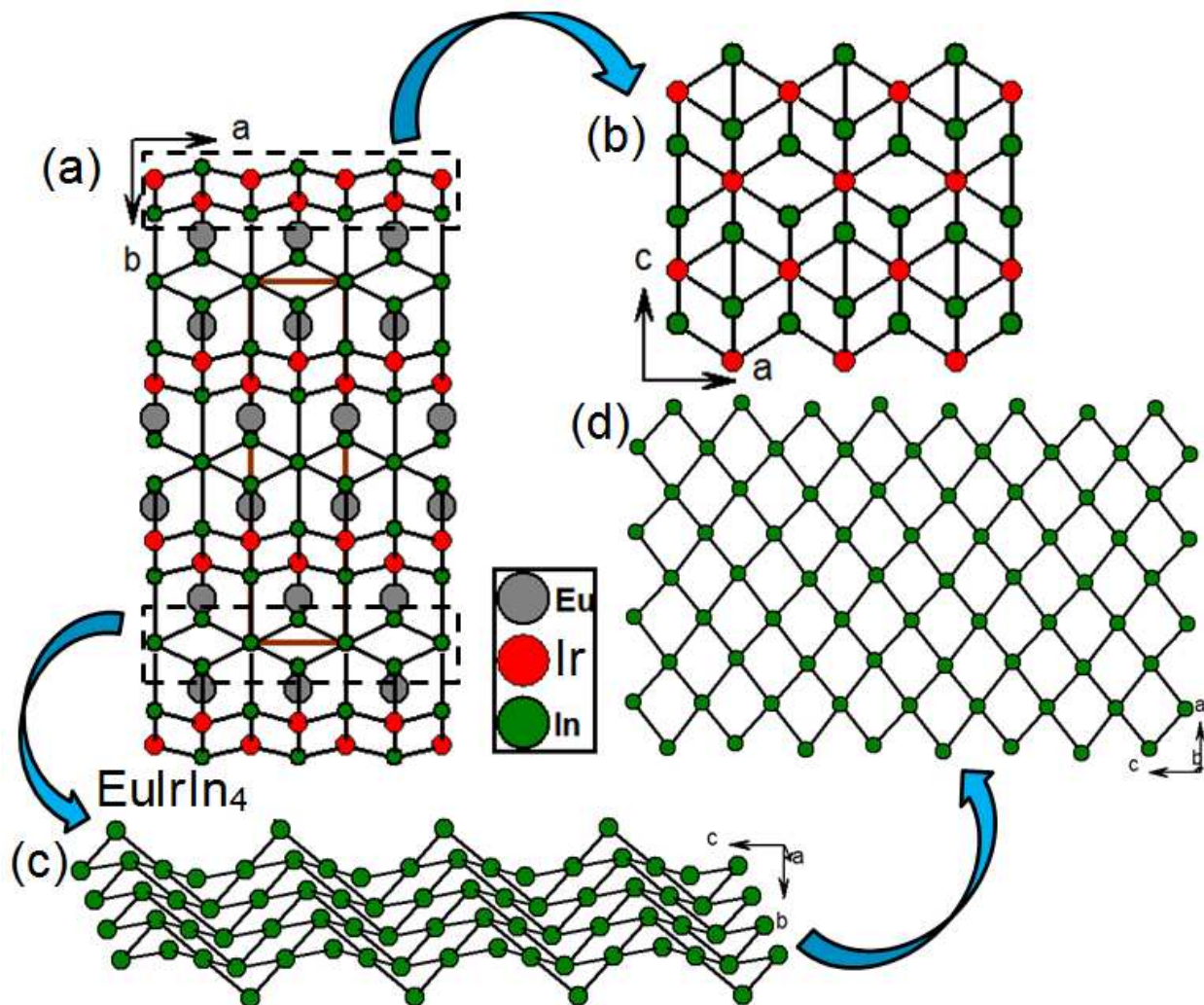
Figure. 2 (a) The unit cell representative of EuIrIn$_4$ viewed along c-axis; (b) zig-zag tetrameric chain constructed from iridium and indium; (c) distorted tetrameric network of indium viewed approximately along bc- plane and (d) b- axis.
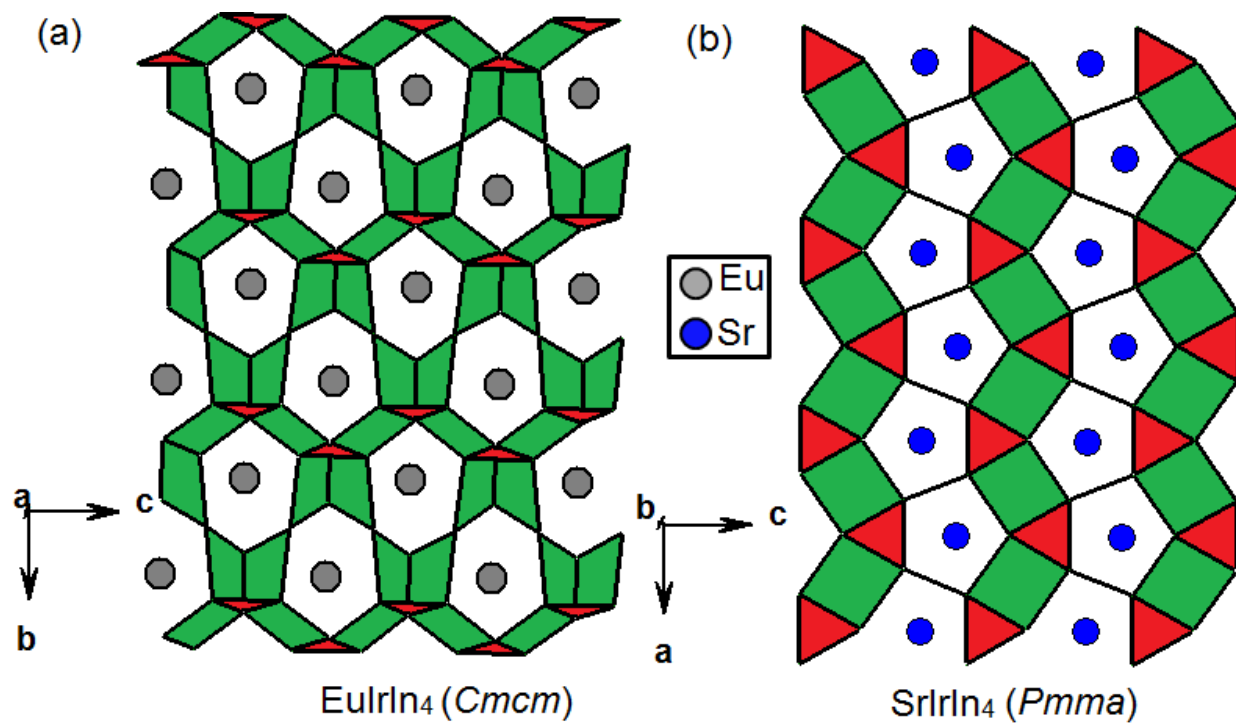
Figure. 3 Comparison between the crystal structures of (a) EuIrIn$_4$ and (b) SrIrIn$_4$ viewed along *a* and *b* -axis respectively.

	Eu (4c)	Ir (4c)	In1 (8f)	In2 (4c)	In3 (4a)
Cmcm (Supercell)	0.0000	0.0000	0.0000	0.0000	0.0000
	0.3751	0.7190	0.1859	0.5652	0.0000
	0.2500	0.2500	0.04830	0.2500	0.0000

$$k2 \begin{bmatrix} a = c' \\ b = a' \\ c = 2b' \end{bmatrix}$$

$$(0, \tfrac{1}{2}, 0)$$

Origin Shift $(0, \tfrac{1}{2}, 0)$

	Sr (2e)	Ir (2e)	In1 (4j)	In2 (2f)	In3 (2a)
Pmma (Subcell)	0.2500	0.2500	0.56644	0.2500	0.0000
	0.0000	0.000	0.5000	0.5000	0.0000
	0.39394	0.81061	0.30951	0.05852	0.0000
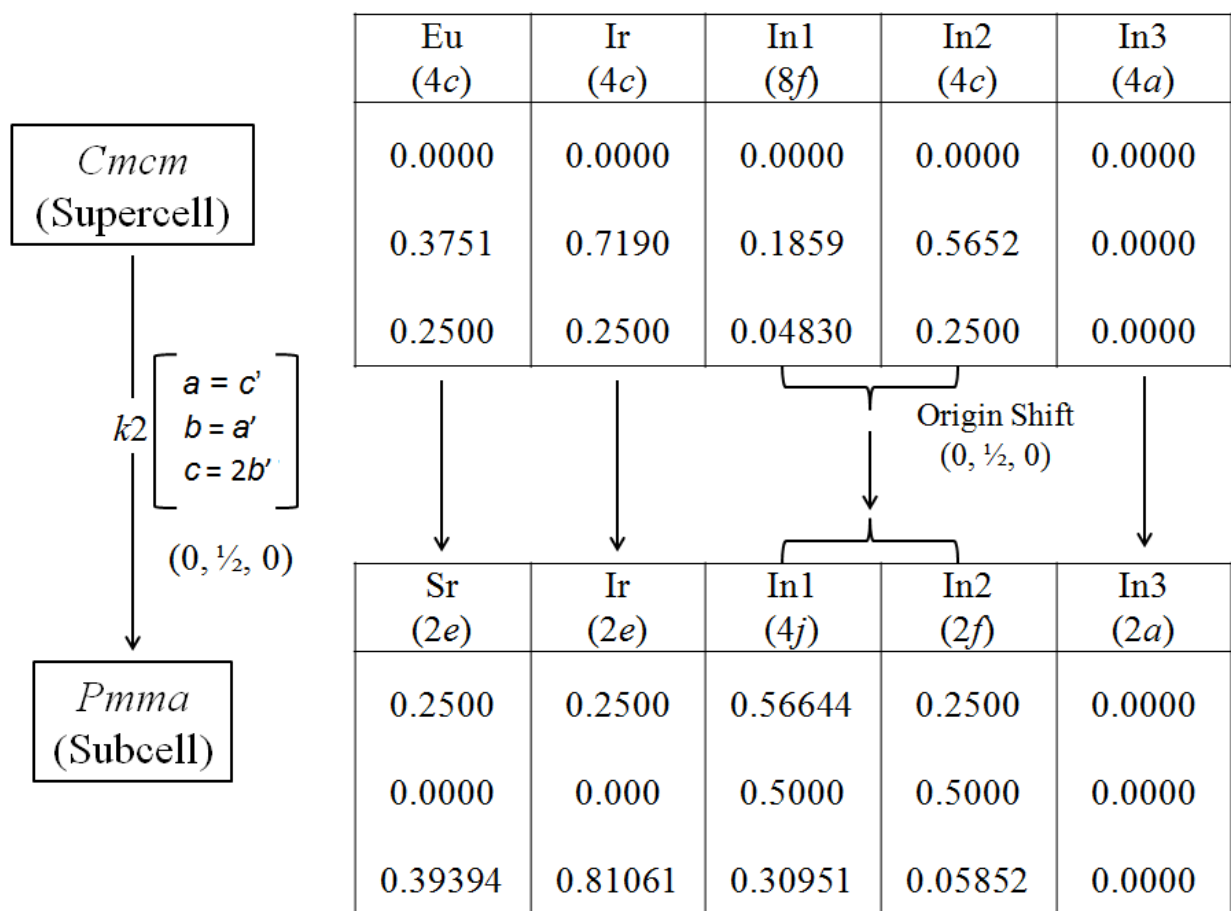
Figure. 4 Group−subgroup scheme of subcell and the superstructure of EuIrIn$_4$. The indices for the klassengleiche (*k*) transition of degree 2 and the unit cell transformations are given. The evolution of the atomic parameters is shown at the right.
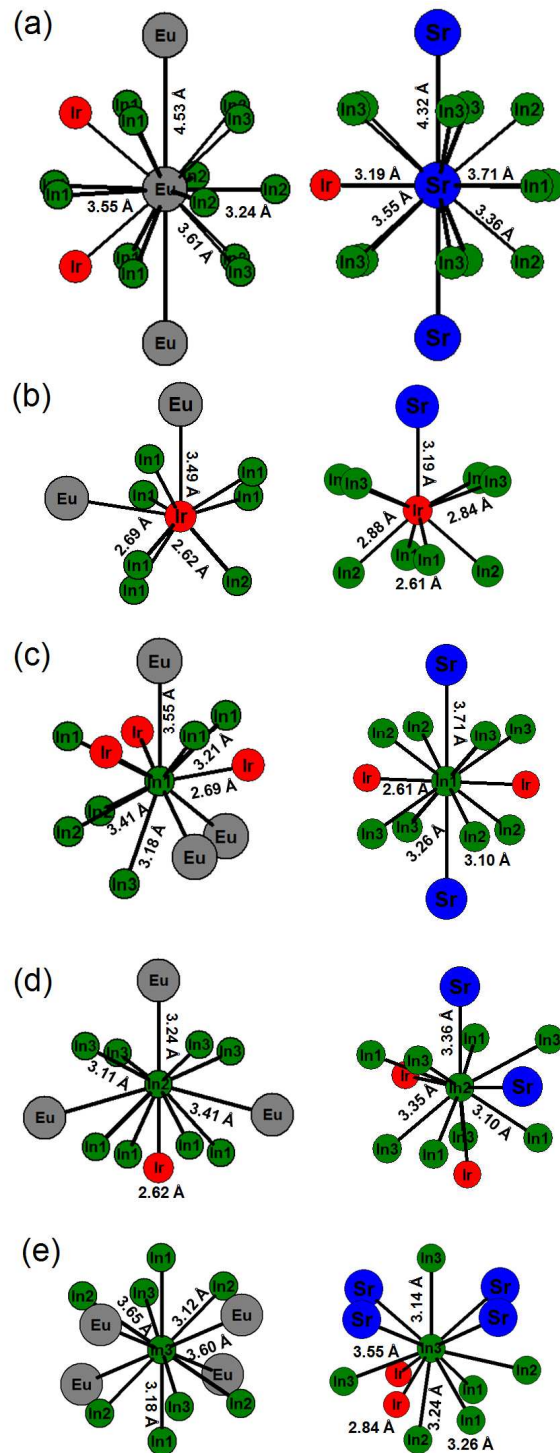
Figure 5. Coordination environment of different atoms in EuIrIn$_4$ and SrIrIn$_4$: (a) Pseudo Frank-Kasper type coordination for Eu and Sr (b) tricapped trigonal prism type coordination for Ir; (c, d, e) Cuboctahedron type coordination for In1, In2 and In3, respectively.
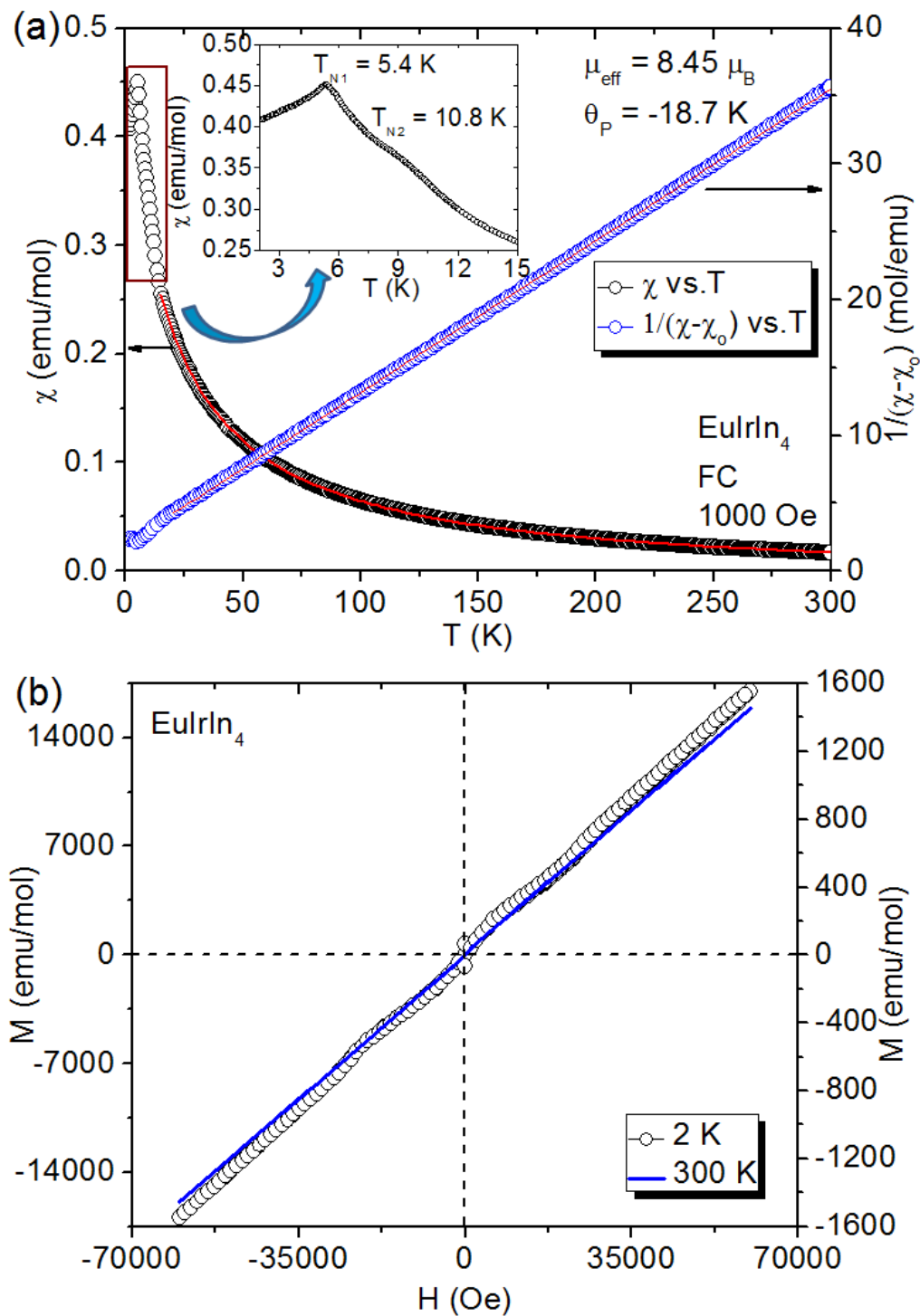
Figure 6. (a) Temperature dependence of magnetic susceptibility and inverse magnetic susceptibility (the inset shows a closer look into the ordering temperature) and (b) field dependence of molar magnetization of EuIrIn₄. The inset in (a) shows the low temperature susceptibility data.
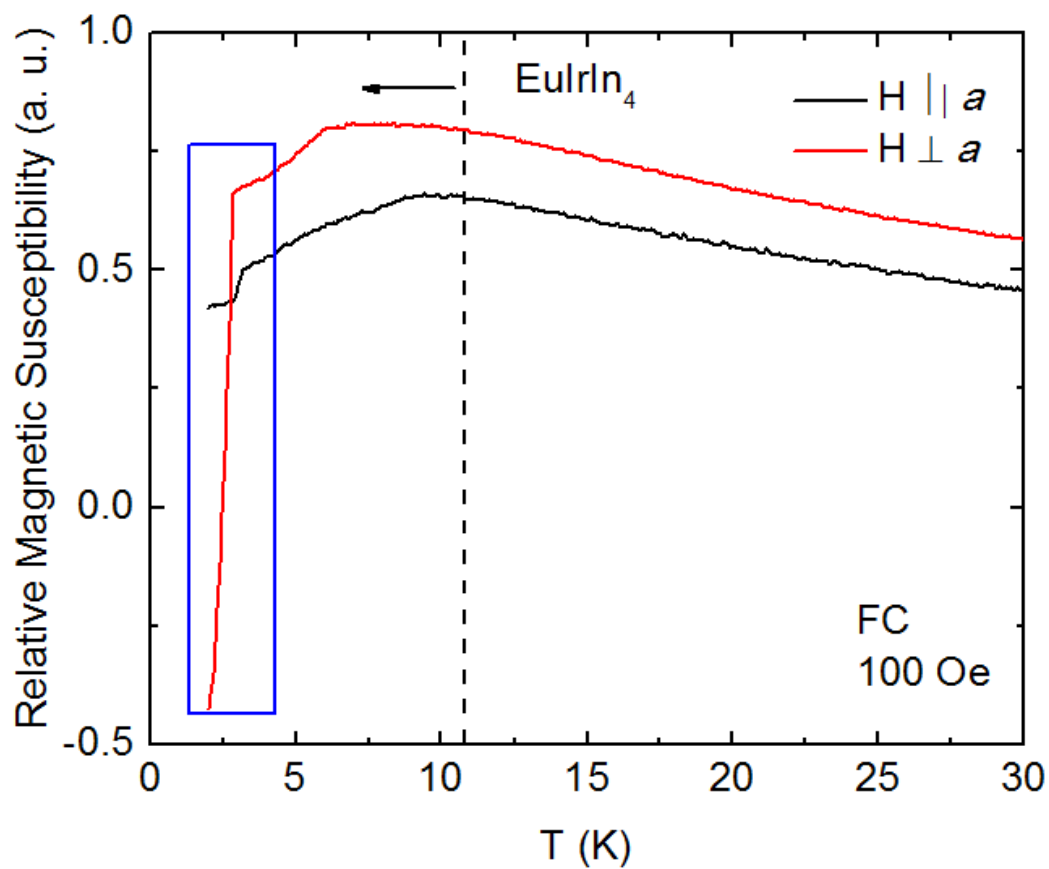
Figure 7. Anisotropic magnetic studies on a EuIrIn$_4$ single crystal; Magnetic field applied parallel and perpendicular to *a*–axis. The blue box shows the demagnetization perpendicular to a-axis. The Dashed line and arrow shows a subtle shift in ordering temperatures.

For The Table of Contents Only
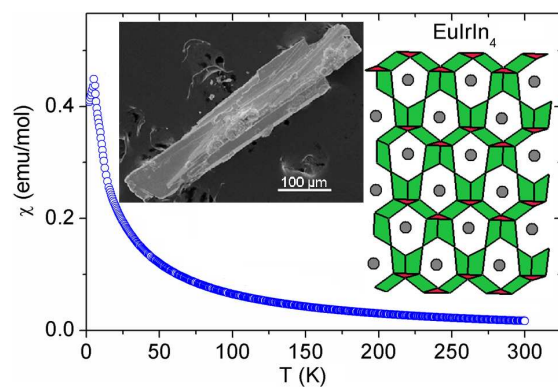
Graphical Abstract

EuIrIn$_4$ is the first member in the Eu-Ir-In family was synthesized by metal flux method using indium as active flux. It is the first YNiAl$_4$ type variant of RETX$_4$ with 9th group transition metals and lanthanides.